This article has been accepted for publication in IEEE Transactions on Geoscience and Remote Sensing. This is the author's version which has not been fully edited and content may change prior to final publication. Citation information: DOI 10.1109/TGRS.2022.3149655

TCNIRv: Topographically-corrected near-infrared reflectance of vegetation for tracking gross primary production over mountainous areas

Rui Chen, Gaofei Yin, *Senior Member*, Wei Zhao, *Senior Member, IEEE*, Baodong Xu, Yelu Zeng, *Member, IEEE*, Guoxiang Liu and Aleixandre Verger

***Abstract*—The near-infrared reflectance of vegetation (NIRv) has been increasingly used as a proxy of gross primary production (GPP) across various temporal scales, ecosystems and climate conditions. However, topography significantly distorts NIRv and GPP estimations over mountainous areas. We evaluated the topographic effects on NIRv and applied a path length correction for improving its performance over mountainous areas. The proposed topographically-corrected NIRv (referred to TCNIRv) was evaluated by multiple Landsat-8 Operational Land Imager images with concurrent *in-situ* GPP measurements over the Lägeren mountainous forest area. TCNIRv reduced topographic effects in the original NIRv and it was comparable to the normalized difference vegetation index (NDVI) and the green normalized difference vegetation index (GNDVI), which are often deemed to be independent of topographic effects. In addition, TCNIRv better agreed with GPP than the other vegetation indices: coefficient of determination R^2 = 0.90 and root mean square error RMSE = 1.40 $gCm^{-2}d^{-1}$ for TCNIRv compared to R^2 = 0.71 and RMSE = 2.47 $gCm^{-2}d^{-1}$ for NIRv. The evaluation shows that TCNIRv is a reliable proxy of GPP, and because of its simplicity and physical soundness, it will facilitate vegetation monitoring over complex topography mountainous areas.**

***Index Terms*—Near-infrared reflectance of vegetation (NIRv), gross primary production (GPP), topographic effects, path length correction (PLC).**

I. INTRODUCTION

Terrestrial gross primary production (GPP), defined as the overall carbon fixation through vegetation photosynthesis, is a key parameter for carbon cycle and climate change research [1, 2]. Mountainous areas occupy a high proportion of the earth's surface and play an important role in the complex Earth system [3]. Therefore, the accurate estimation of GPP over mountainous areas is essential to understand the terrestrial ecosystems and global carbon balance.

Over the past several decades, various satellite data-driven models have been proposed to estimate GPP. They can be primarily divided into two categories: (1) ecosystem mechanistic and (2) empirical statistical models. The ecosystem mechanistic models mainly incorporate process-based [4] or light use efficiency models [5]. However, they require meteorological data, which are often not available over mountainous areas, because of the scarce distribution of weather stations therein [6, 7]. In those cases, statistical models based on empirical relationships between field-measured GPP and vegetation indices (VIs) provide an alternative to estimate GPP over mountainous areas.

The selection of appropriate VIs is the prerequisite of statistical models to estimate GPP. Among the existing VIs, the normalized difference vegetation index (NDVI) is the most widely used VI as a proxy for GPP [8-10]. However, many confounding factors, e.g., atmospheric conditions, soil background and saturation effects, strongly influence its value [11] and hinder its applications. NDVI is known to be insensitive to GPP at high leaf area index (LAI) values and it is not recommended for tracking the phenology of GPP during the senesce when canopy greenness and physiology are decoupled [12, 13]. Therefore, many VIs have been developed to overcome these limitations. Among them, chlorophyll-sensitive VIs such as the green NDVI (GNDVI), which uses the green band instead of the red band which is used in NDVI, appears to better correlate with LAI and GPP phenology [14]. The near-infrared reflectance of vegetation (NIRv), which represents the near-infrared reflectance of vegetation component of the pixel,

The work was partially supported by the National Natural Science Foundation of China (Grant No. 41971282, 42001303), and Sichuan Science and Technology Program (2021JDJQ0007; 2020JDTD0003), and the European Union's Horizon 2020 research and innovation programme under the Marie Sklodowska-Curie grant agreement (No. 835541). (*Corresponding author: Gaofei Yin, Guoxiang Liu.*)

R. Chen and G. Yin are with the Faculty of Geosciences and Environmental Engineering, Southwest Jiaotong University, Chengdu 610031, China (e-mail: yingf@swjtu.edu.cn).

W. Zhao is with the Institute of Mountain Hazards and Environment, Chinese Academy of Sciences, Chengdu 610041, China.

Y. Zeng is with the Department of Global Ecology, Carnegie Institution for Science, Stanford, CA 94305, USA.

B. Xu is with the Macro Agriculture Research Institute, College of Resources and Environment, Huazhong Agricultural University, Wuhan 430070, China.

G. Liu is with the Faculty of Geosciences and Environmental Engineering, Southwest Jiaotong University and the State-Province Joint Engineering Laboratory of Spatial Information Technology for High-Speed Railway Safety, Chengdu 610031, China (e-mail: rsgxliu@swjtu.edu.cn).

A. Verger is with the Desertification Research Centre CIDE-CSIC, València 46113, Spain, and with CREAF-CSIC-UAB, Cerdanyola del Vallès 08193, Catalonia, Spain.

This article has been accepted for publication in IEEE Transactions on Geoscience and Remote Sensing. This is the author's version which has not been fully edited and content may change prior to final publication. Citation information: DOI 10.1109/TGRS.2022.3149655

has also been demonstrated as a robust proxy of GPP [15, 16]. NIRv minimizes the effects of background contamination [15, 17] and the saturation effects at high biomass regions [16], but it is very sensitive to topographic effects [18].

In mountainous areas, topography modifies the local surface illumination conditions [19], canopy structure [20, 21] and sun-target-sensor geometry, and significantly affects canopy bidirectional reflectance distribution function characteristics. NDVI and GNDVI mediate the topographic effects because of their normalized difference formula. On the contrary, NIRv and NIRv-derived estimates of vegetation biophysical and biochemical parameters are associated with considerable uncertainties over mountainous areas [18]. However, to the best of our knowledge, NIRv-GPP relationship over mountainous areas has not been systematically evaluated. Hence, it is essential to further evaluate topographic effects on NIRv and minimize their influence for accurate estimation of GPP.

A series of topographic correction methods have been proposed in the last decades, e.g., C-correction [22], statistical-empirical (SE) [22], sun-canopy-sensor (SCS) [23], Dymond-Shepherd (D-S) [24] and sun-canopy-sensor with C-correction (SCS + C) [25]. These methods generally rely on empirical parameters acquired through regression between remote sensing observations and topographic factors. Therefore, although they perform excellent for images at single phases [26, 27], inconsistency occurs in time series and spatial mosaic applications due to the temporally and spatially specific nature of the empirical parameters [28, 29]. On contrary, path length correction (PLC) is a physically-based topographic correction method, which was deduced from the simplification of the radiative transfer equation [27]. The mechanism underlying the PLC is that topography would stretch/compress the photon traveling distance (path length) within canopy in up-/down-slope direction, therefore, the topographic effects could be reduced through compensating photon path length distortion [21, 30]. PLC provides a new paradigm to support long-term and large-scale vegetation monitoring over mountainous areas [29].

The main objective of this study is to propose a topography-insensitive NIRv to support GPP tracking over mountainous areas. Specific objectives are: (1) to evaluate the topographic effects on the NIRv; (2) to propose a topographically-corrected NIRv (TCNIRv) through PLC; (3) to validate the performance of the proposed TCNIRv in GPP estimation over mountainous areas. The topographic effects on TCNIRv and its performance for tracking GPP are compared with the original NIRv and with the supposed topographic independent NDVI and GNDVI indices. This paper is organized as follows. The background theory for NIRv and PLC, and the derivation of TCNIRv are described in Section II, the experimental setup in Section III and results in Section IV. Finally, discussion and conclusion are presented in Sections V and VI.

II. METHODS

A. Theoretical Background

The proposed TCNIRv was derived by a combination of NIRv and PLC methods. Details can be found in [17] and [27], respectively. We only provide brief explanations here:

1) Near-infrared Reflectance of Vegetation (NIRv)

NIRv represents the near-infrared band reflectance from only the vegetation component [16, 17]. It is defined as [17]:

$$NIRv = NDVI \cdot NIR \tag{1}$$

$$NDVI = \frac{NIR - R}{NIR + R} \tag{2}$$

where R and NIR represent the red and near-infrared reflectances, respectively, and NDVI represents the normalized difference vegetation index.

NDVI and NIR vary with the soil brightness in an opposite manner: darker soils have a higher NDVI but lower NIR, while brighter soils have a lower NDVI but higher NIR [31]. Therefore, NIRv, as the product of NDVI and NIR, can effectively addresses the soil background influence and mixed-pixel problem. Compared with many other VIs, NIRv also exhibits less saturation phenomenon for dense vegetation [16].

2) Path Length Correction

According to path length correction (PLC) method [27], the reflectance over a slopped surface (ρ_O) can be converted to its horizontal equivalent (ρ_{PLC}) by multiplying a topographic normalization conversion factor (P):

$$\rho_{PLC} = P \times \rho_O \tag{3}$$

$$P = \frac{S(\Omega_1) + S(\Omega_2)}{S_t(\Omega_1) + S_t(\Omega_2)} \tag{4}$$

where Ω_1 and Ω_2 are the solar and viewing directions, respectively. S and S_t, respectively, are the path lengths over the horizontal and slopped surfaces, which can simply be calculated as:

$$S(\theta) = 1/\cos\theta \tag{5}$$

$$S_t(\theta, \varphi, \alpha, \beta) = \frac{1}{\cos\theta\left(1 - \tan\alpha\cos(\varphi - \beta)\tan\theta\right)} \tag{6}$$

where θ and φ are the zenith and azimuth angles for the solar or viewing direction, respectively. α and β are the slope and aspect of the slopped terrain, respectively. Note that the normalization conversion factor was derived through the simplification of the classic radiative transfer equation under the assumption that the observed reflectance is only from vegetation [27].

B. TCNIRv Formulation

NIRv represents the near-infrared band reflectance from vegetation component exclusively [17] and the contribution of soil to the pixel scale reflectance is eliminated (Eq. 1). Consistently, for deriving the conversion factor (P, see Eq. (3)), PLC assumes that the radiance collected by the sensor is only from the vegetation [27], and neglects the soil contamination. The physical meaning of the reflectance in NIRv and in PLC is identical. This makes the direct combination between them possible, and therefore we propose the following simple yet physically sound topographically corrected NIRv (TCNIRv):

$$TCNIRv = NIRv \cdot P \tag{7}$$

where NIRv and P are the near-infrared reflectance of vegetation and topographic normalization conversion factor, which can be calculated from Eq (1) and Eq (4), respectively. The proposed TCNIRv, by nature, represents the equivalent near-infrared reflectance of vegetation (without soil contamination) over flat terrain, which is under identical

This article has been accepted for publication in IEEE Transactions on Geoscience and Remote Sensing. This is the author's version which has not been fully edited and content may change prior to final publication. Citation information: DOI 10.1109/TGRS.2022.3149655

structural and leaf characteristics as its topographic influenced NIRv counterpart.

III. EXPERIMENTAL SETUP

A. Study Areas

Two 30 km × 30 km mountainous regions, with contrasting topographies, were selected (Fig. 1). The terrain in the study area I (centered at 47°58′ N and 6°59′ E) has a complex orography with the elevation ranging from 305 to 1419 m, and its dominant land-cover type is forest. The study area II (centered approximately 47°28′ N and 8°21′ E) is located in a terrain with a simple orography with an elevation ranging from 298 to 876 m, and it has varying land-cover types, including cropland, forest, and urban settlement. The two study areas are characterized by a typical oceanic climate.

The Lägeren forest flux site (CH-Lae) located in the center of the study area II (the white triangle in Fig. 1) was also selected to evaluate the performance of TCNIRv in capturing the GPP dynamics. This site is located on a south facing slope of the Jura Mountain, and its altitude and slope are 682 m and 27°, respectively [32]. The dominant land cover around the CH-Lae flux site is mixed deciduous forest, with the mean tree height around 30 m [32].

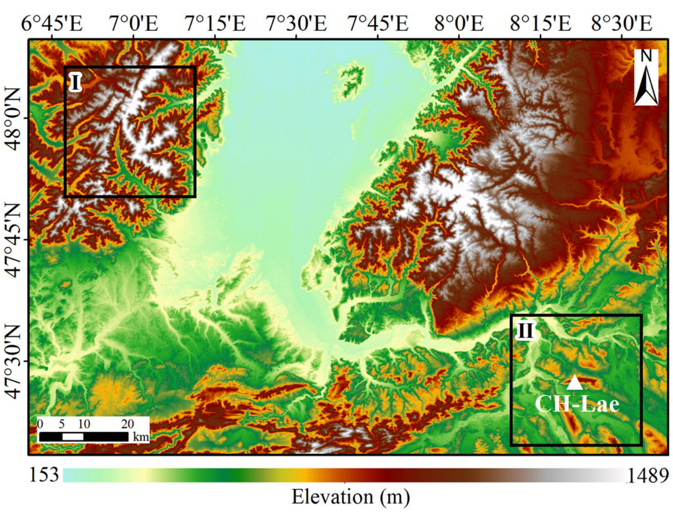

Fig. 1. AW3D30 elevation map with indication of the study areas I and II. The white triangle in study area II refers to the location of CH-Lae flux tower site.

B. Data

1) Flux Data: The daily GPP estimations (GPP_NT_VUT_REF) at CH-Lae flux tower from 2014 through 2018 were employed to analyze whether TCNIRv can improve the capacity of NIRv in tracking GPP over mountainous areas. The nighttime partitioning method was used to generate the GPP estimates. The latest FLUXNET2015 Tier 1 dataset (Pastorello et al. 2020) freely available at https://fluxnet.fluxdata.org was used. Before analysis, we firstly smoothed the daily GPP time-series through adaptive Savitzky-Golay (SG) filtering [33] to reduce the bias introduced by random noise. The width of the moving window determines the degree of smoothing, and therefore is a crucial parameter of the SG filtering [34]. A rough guide value is around a quarter of the length of the annual time series [35], and thus was set to 90 days in this study.

2) Landsat-8 OLI Data: We downloaded all the surface reflectance (L2A) Landsat-8 Operational Land Imager (OLI) images spanning 2014 through 2018 (i.e., 38 and 58 images for study areas I and II, respectively) from Google Earth Engine (GEE) [36]. These GEE products were already atmospherically corrected based on the Land Surface Reflectance Code (LaSRC) [37]. The snow, cloud and cloud shadow contaminated observations were filtered out according to the data quality layer [38].

3) Digital Elevation Model Data: The Advanced Land Observing Satellite global digital surface model (AW3D30), based on optical stereo matching of the Panchromatic Remote-sensing Instrument for Stereo Mapping (PRISM) images [39], was also employed in this study. Its spatial resolution is 1 arc-second (approximately 30 m) with a height accuracy of 4.40 m (RMSE) [40]. The AW3D30 dataset was released at https://www.eorc.jaxa.jp/ALOS/en/aw3d30/data/index.htm by the Japan Aerospace Exploration Agency. Based on this dataset, topographic parameters, including slope and aspect, were calculated to implement topographic correction.

C. Evaluation Methodology

We assumed that a good VI, suitable for tracking GPP over mountainous areas, should be independent from topography and strongly correlated with GPP. Therefore, TCNIRv was evaluated in two aspects: (1) whether it can reduce the topographic effects; and (2) whether it can capture the GPP dynamics in mountainous areas.

Three VIs, including the original NIRv, the NDVI and the GNDVI were selected for comparison. NDVI (Eq. 2) was found nearly insensitive to topography [41], and NIRv (Eq. 1) was often seen as a reliable proxy for GPP [15, 17, 42]. GNDVI, formulated as

$$GNDVI = \frac{NIR - G}{NIR + G} \tag{8}$$

where G represents the green reflectance, was sensitive to chlorophyll content [43], and should, in theory, be a good proxy for GPP. Besides, GNDVI was insensitive to topography due to its normalized difference formula.

The most widely used topographic correction evaluation method, i.e., correlation analysis [26], was adopted in this study. It used the determination coefficient (referred to R^2_{TC} hereafter), between the cosine of local solar incident angle ($\cos(i)$) and the VI, as a criterion to quantify the topographic effects on VIs. The $\cos(i)$ is calculated as

$$\cos(i) = \cos(\alpha)\cos(\theta_s) + \sin(\alpha)\sin(\theta_s)\cos(\varphi_s - \beta) \tag{9}$$

where α and β are slope and aspect, respectively, which are derived from the DEM. θ_s and φ_s are the solar zenith and azimuth angles of the OLI images, respectively [22, 25]. An ideal topography-insensitive VI will have a R^2_{TC} value close to zero. Note that all pixels at 30 m resolution of study area I/II were collected to calculated R^2_{TC} over time.

In addition, we also analyzed the temporal consistency between GPP and VIs at the CH-Lae flux tower site. To minimize the mismatch of the footprint between the GPP

This article has been accepted for publication in IEEE Transactions on Geoscience and Remote Sensing. This is the author's version which has not been fully edited and content may change prior to final publication. Citation information: DOI 10.1109/TGRS.2022.3149655

measurement and Landsat-8 derived VIs, the VI values were averaged in a 300 m × 300 m sampling window around the CH-Lae site to compare with field measured GPP. To assess the capacity of VIs to predict GPP, the field measured GPP at the date of Landsat-8 acquisition were used as a reference. A linear regression between each VI and field GPP was established to retrieve GPP form Landsat-8 data. Finally, the performance of the VI-derived GPP was assessed using the determination coefficient (R^2) and the root mean square error (RMSE) as compared with *in-situ* GPP.

IV. Results

A. Topographic Effects on VIs

A.1. Temporal Dependence of Topographic Effects

Fig. 2 shows the temporal change in R^2_{TC} from 2014 to 2018 for study area I and II. Strong fluctuations were observed for NIRv, and the largest R^2_{TC} values appeared during winter and early spring (R^2_{TC} up to 0.65 and 0.4 for study area I (Fig. 2(a)) and II (Fig. 2(b)), respectively) when the solar zenith angle values are the highest (Fig. A1, see Appendix). The GNDVI also showed high R^2_{TC} values and strong seasonal fluctuations over study area II. In contrast to NIRv and GNDVI, NDVI and TCNIRv showed low R^2_{TC} values and were relative stable throughout the study period for the two study areas. For a better comparison, the average R^2_{TC} values throughout the study period for NDVI (≈0.027/0.024 for study area I/II), GNDVI (≈ 0.038/0.006), NIRv (≈ 0.110/0.300) and TCNIRv (≈ 0.021/0.013) also were depicted in Fig. 2. The results showed that the TCNIRv was comparable to NDVI in reducing topographic effect. Closer inspection revealed that TCNIRv was slightly more stable across time than NDVI.

A.2. Spatial Dependence of Topographic Effects on VIs

Most existing studies relying on NIRv to capture GPP variations were implemented at coarse resolution (lower than 1 kilometer) [15, 42] for which topographic effects may be safely ignored. However, topographic effects are resolution-dependent [3]. We simulated the resolution-dependence of topographic effects on VIs through aggregating Landsat-8 observations for study area II (Fig. 3). Results show that the topographic effects caused by shadows and micro-slopes were higher across different scales for NIRv than for TCNIRv, NDVI and GNDVI. The topographic effects on NIRv gradually decreased from 0.247 to nearly zero when observations were aggregated from decametric to kilometric resolutions. This highlights the necessity of a topographic correction for NIRv specially at the high spatial resolution. In contrast to NIRv, the topographic effects on NDVI, GNDVI and TCNIRv were marginal and insensitive to spatial resolution, i.e., they provide consistent results across varying resolutions over mountainous areas.

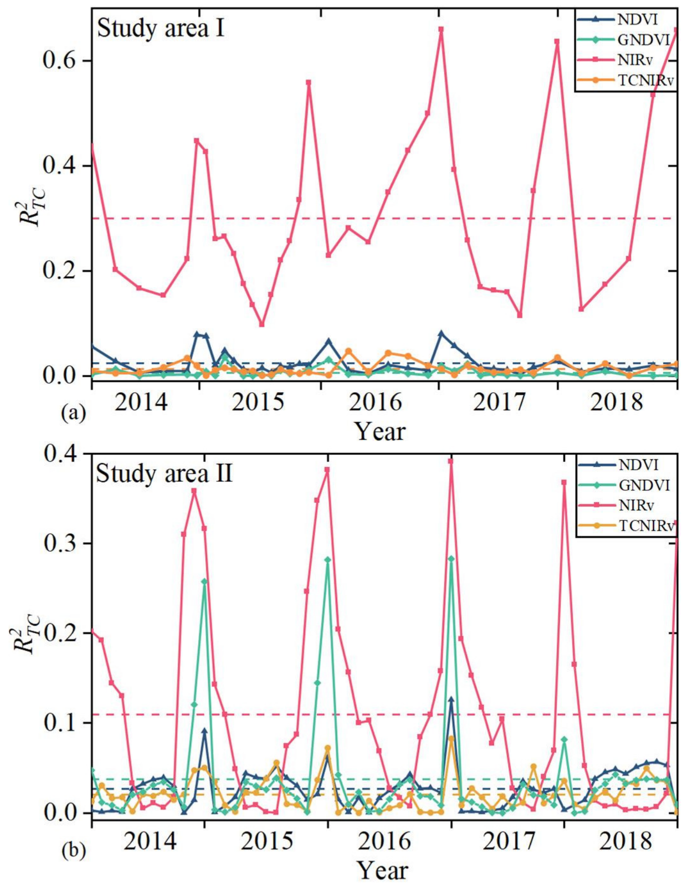

Fig. 2. The temporal profile of the determination coefficient (R^2_{TC}) between the vegetation indices (i.e., the normalized difference vegetation index (NDVI), the green normalized difference vegetation index (GNDVI), the near-infrared reflectance of vegetation (NIRv), and the proposed topographically-corrected NIRv (TCNIRv)) and the cosine of the local solar incidence angle (cos(i)) for the study areas (a) I and (b) II. The dashed lines represent the average R^2_{TC} values for the entire period.

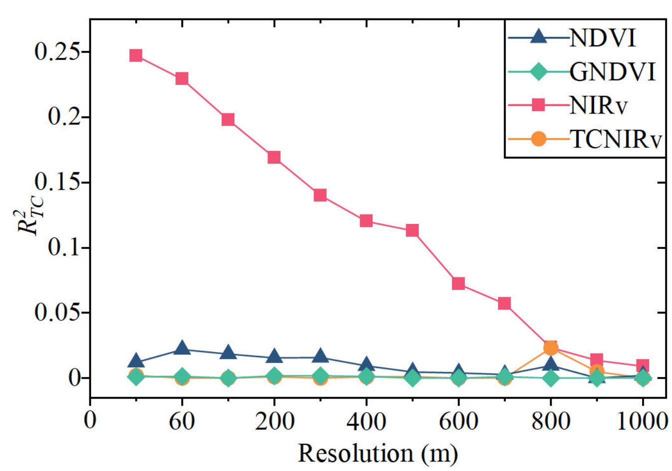

Fig. 3. Spatial dependence of the determination coefficient (R^2_{TC}) between the vegetation indices (i.e., the normalized difference vegetation index (NDVI), the green normalized difference vegetation index (GNDVI), the near-infrared reflectance of vegetation (NIRv), and topographically-corrected NIRv (TCNIRv)) and the cosine of the local solar incidence angle (cos(i)). Assessment based on aggregating the OLI image acquired over study area II on October 1st, 2015, from decametric to kilometric spatial resolutions.

This article has been accepted for publication in IEEE Transactions on Geoscience and Remote Sensing. This is the author's version which has not been fully edited and content may change prior to final publication. Citation information: DOI 10.1109/TGRS.2022.3149655

B. Correlation with In-situ GPP Measurements

B.1. Temporal Dependence of GPP-VIs Relationship

NDVI, GNDVI, NIRv and TCNIRv all followed the general GPP dynamics (Fig. 4). However, closer inspection revealed that, during peak growing season, the dynamic ranges of NDVI and GNDVI (Fig. 4(a) and (b)) are narrower than NIRv and TCNIRv (Fig. 4(c) and (d)), because of the saturation effect. Meanwhile, NDVI and GNDVI still were relative stable with the large values when GPP started to decrease. The desynchronization of NDVI and GNDVI with GPP indicated the difficulties of these indices to track GPP phenology in the senescence period. It is also noteworthy, NIRv was generally lager due to stronger topographic effects in winter (see Fig. 2), therefore it was difficult to capture GPP dynamics. In contrast, TCNIRv had the best synchronization with GPP throughout the study period.

Scatter plot between VIs and GPP also exhibited the saturation effect on NDVI and GNDVI (see Fig. 5(a) and (b)): NDVI and GNDVI keep a relative stable value (~0.9 and ~0.8) when GPP is larger than 9 $gCm^{-2}d^{-1}$. This saturation effect was obviously reduced for NIRv and TCNIRv (Fig. 5(c) and (d)). The proposed TCNIRv showed the strongest linear relationship with GPP (R^2 = 0.90, RMSE = 1. 40 $gCm^{-2}d^{-1}$) and improved NIRv (R^2 = 0.71, RMSE = 2.47 $gCm^{-2}d^{-1}$), NDVI (R^2 = 0.63, RMSE = 2.77 $gCm^{-2}d^{-1}$) and GNDVI (R^2 = 0.60, RMSE = 2.88 $gCm^{-2}d^{-1}$) performances when evaluated over the entire study period. We further evaluated the performances of VIs specifically over the growing season from April through August. The results showed that the proposed TCNIRv still had the strongest linear relationship with GPP over the growing season (R^2 of 0.85, 0.63, 0.50 and 0.52 for TCNIRv, NIRv, NDVI and GNDVI, respectively).

B.2. Spatial Dependence of GPP-VIs Relationship

The validation results from direct comparison with flux-based GPP is influenced by the scale dependency of topographic effects but also by the spatial representativeness of eddy covariance flux footprints. Fig. 6 and 7 respectively show the sampling size-dependent variation of R^2 and RMSE (between VIs and *in-situ* GPP). Results showed R^2 (RMSE) for NDVI, GNDVI and NIRv increased (decreased) with the sampling size. In contrast, TCNIRv was relative stable across sampling sizes with the highest R^2 (~0.9) and lowest RMSE (~1.5 $gCm^{-2}d^{-1}$). All VIs had a relatively good consistency with GPP at the kilometric scale, because the topographic effects were mitigated (see Fig. 3). The specified sampling size of 300 m selected here for the validation and recommended also by [44] appears suitable to capture both the spatial representativeness of GPP and topographic effects simultaneously.

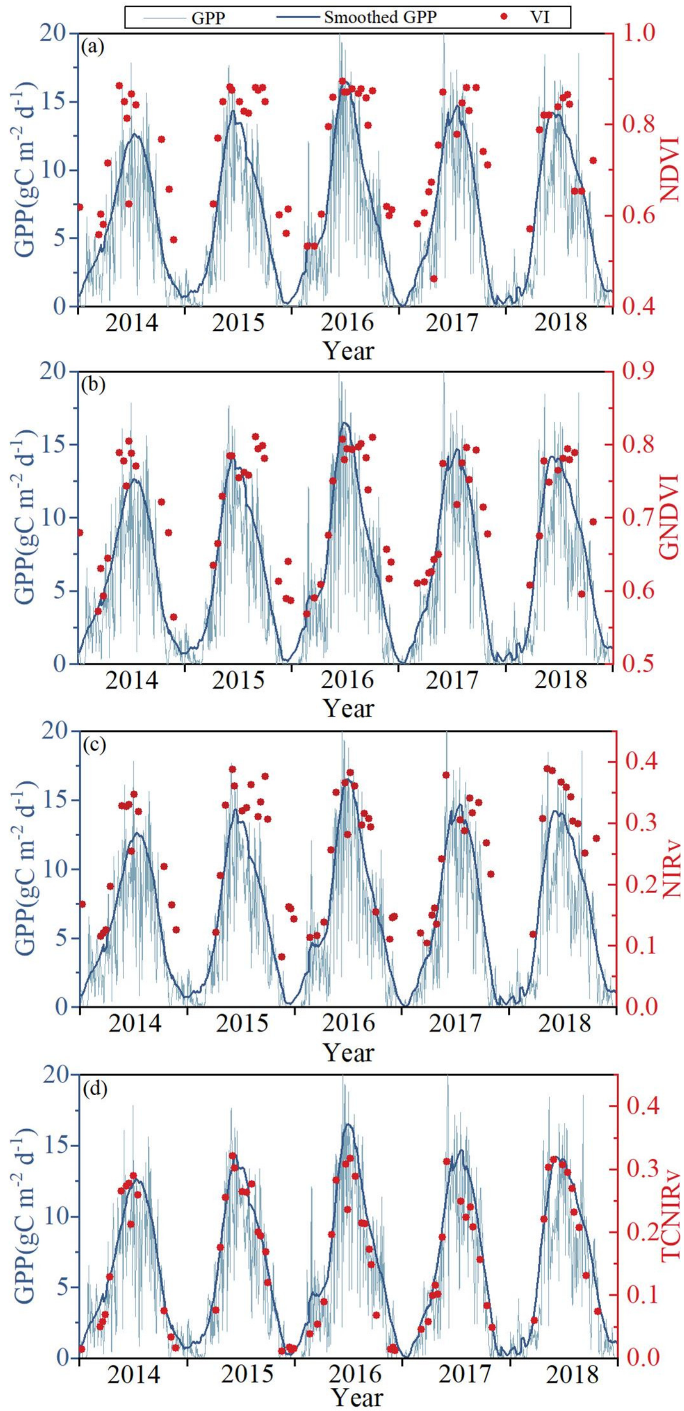

Fig. 4. Temporal profile of field measured GPP and different vegetation indices: (a) the normalized difference vegetation index (NDVI), (b) the green normalized difference vegetation index (GNDVI), (c) the near-infrared reflectance of vegetation (NIRv) and (d) the topographically-corrected NIRv (TCNIRv), over the CH-Lae site.

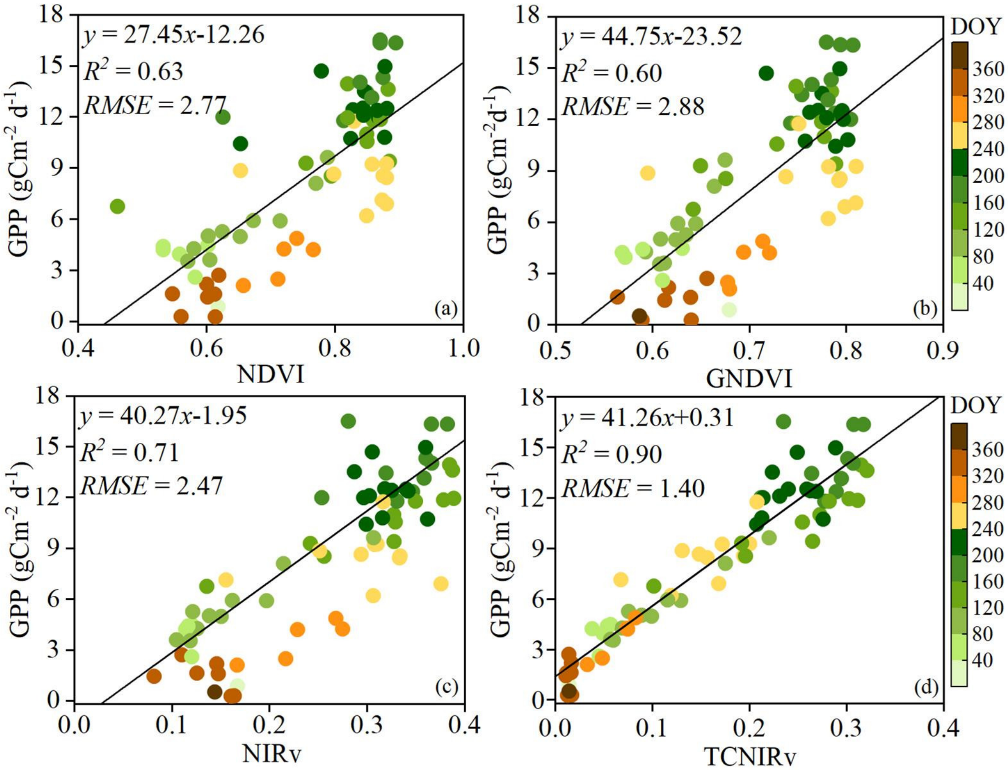

Fig. 5. Relationships between *in-situ* GPP and different vegetation indices: (a) the normalized difference vegetation index (NDVI), (b) the green normalized difference vegetation index (GNDVI), (c) the near-infrared reflectance of vegetation (NIRv) and (d) the topographically-corrected NIRv (TCNIRv). Assessment over the CH-Lae site. The solid lines indicate fitted regression lines between GPP and VIs. The different colors represent the day of year (DOY).

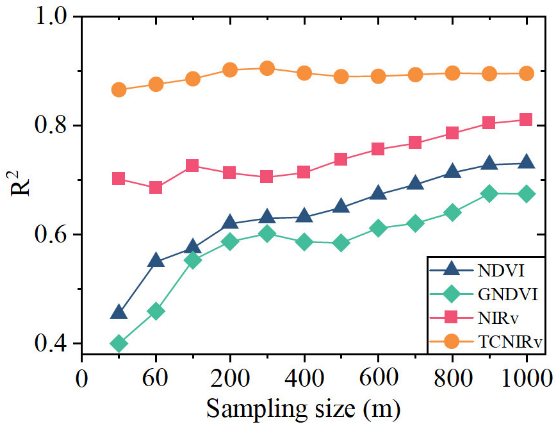

Fig. 6. Spatial dependence of the determination coefficient (R^2) between *in-situ* GPP and the vegetation indices (i.e., the normalized difference vegetation index (NDVI), the green normalized difference vegetation index (GNDVI), the near-infrared reflectance of vegetation (NIRv), the topographically-corrected NIRv (TCNIRv)) at different sampling size from decametric to kilometric spatial resolutions.

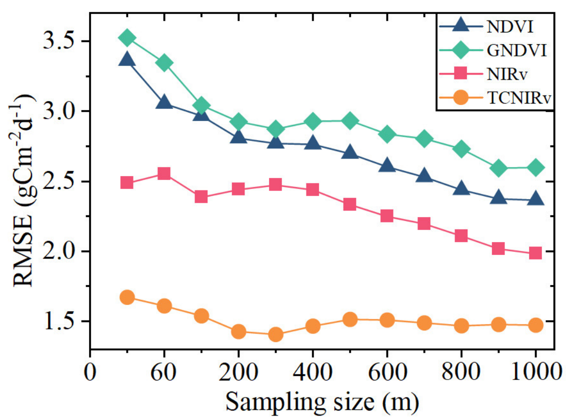

Fig. 7. Spatial dependence of the root mean square error (RMSE) between *in-situ* GPP and the vegetation indices (i.e. the normalized difference vegetation index (NDVI), the green normalized difference vegetation index (GNDVI), the near-infrared reflectance of vegetation (NIRv), the topographically-corrected NIRv (TCNIRv)) at different sampling size from decametric to kilometric spatial resolutions.

V. Discussion

Over mountainous areas, the obvious spatial heterogeneity, such as the steep slopes and radiation variations, makes GPP estimation more challenging. Among the existing models, detailed ecosystem mechanistic models can provide excellent fits to flux site data when accurately parameterized [45]. However, the scarcity of accurate meteorological data over mountainous areas makes the parameterization of ecosystem mechanistic models a very difficult task. Therefore, the routinely monitoring of GPP with ecosystem mechanistic models is still infeasible over our mountainous areas [6].

The availability of long-term satellite observations has made it more direct and convenient to estimate GPP entirely from remotely sensed data. The simplest models explore the correlation between GPP and VIs. The most widely used NDVI saturates easily for dense vegetation [41], and thus has a poor performance in tracking GPP for high LAI values. Our findings show the limitation of NDVI for capturing GPP at the peak of vegetation season. NDVI evidences also important limitations to track GPP in the Lägeren deciduous forest during the senescence period as we reported in previous studies [13] GNDVI, which has similar formula to NDVI by replacing the red by the green spectral band, is sensitive to chlorophyll content [43]. Therefore, it is supposed to be a better proxy for GPP. However, our results showed that GNDVI performed slightly worse than NDVI in the comparison with GPP (R^2 = 0.60/0.63 and RMSE = 2.88/2.77 for GNDVI/NDVI, see Fig. 5(a) and (b)). This may be explained because of the stronger atmospheric contamination in the green band due to Rayleigh scattering than in the red band. The strong atmosphere-land interaction over mountainous areas further exacerbates the atmospheric contamination in green band [29]. Baldocchi *et al.* [16] demonstrated that NIRv was a reliable proxy for GPP compared to others VIs. Our results corroborate it but highlights the importance of a topographic correction for mountain areas. Direct comparison between TCNIRv and NIRv (Fig. 8) shows that TCNIRv has lower values over the sun-ward CH-Lae site, and their discrepancy was dependent on the illumination condition of the sloped surface (represent by cos(i)): the higher the solar zenith angle (i.e., the smaller cos(i)) the larger the differences. Considering that high solar zenith angle causes more obvious topographic effects (see Fig. 2 and A1), TCNIRv is capable of self-adaptively mediating the topographic effect according to their magnitude.

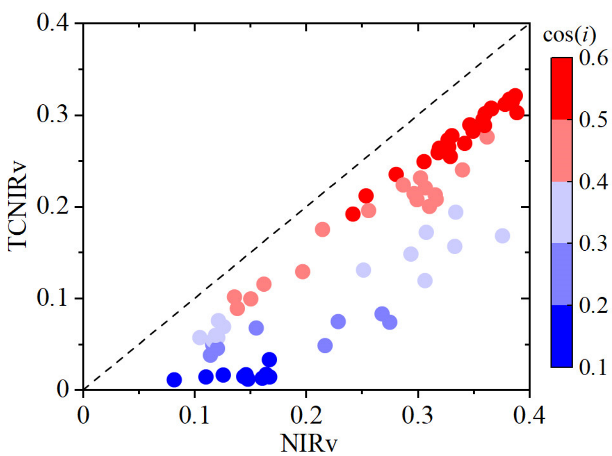

Fig. 8. Comparison of the near-infrared reflectance of vegetation (NIRv) and the topographically-corrected NIRv (TCNIRv) as a function of the cosine of the local solar incidence angle (cos(i)) over the CH-Lae site. The dashed line is the 1:1 line.

Many topographic correction methods have been proposed in early studies, e.g., C-correction [22], SE [22] and SCS+C [25]. However, those topographic correction methods were dedicatedly designed for reflectances. Meanwhile, the empirical parameters in those correction methods are temporally and spatially specific, which is not conducive to vegetation monitoring at long term and large areas [28]. Therefore, the common strategy to obtain topography-insensitive VIs, i.e., first correct reflectance through above-mentioned methods (e.g., C, SE, and SCS+C) and then calculate VIs, might not be the best choice for operational implementation [18]. An alternative strategy is to directly develop VIs independent from topographic effects. For example, Liao *et al.* [46] modified the EVI by changing the soil adjustment index from a constant to a variable related to the cos(i), extending the applicability of EVI to mountainous areas. However, this modified EVI still has an empirical nature. Contrary to exiting studies, the proposed TCNIRv in this study has solid mechanism basis without any empirical parameter. In addition, TCNIRv has a very simple formulation, benefiting the operational use in vegetation monitoring at a large spatio-temporal scale.

In this work, we analyzed the capacity of the VIs (NDVI, GNDVI, NIRv and the proposed TCNIRv) to capture the GPP dynamics with flux-based measurements as a benchmark (Fig. 4 and 5). Note that flux-based GPP measurements *per se* are influenced by topography, because the steady-condition assumption underlying the eddy covariation technique does not always hold over mountainous areas [47]. The uncertainty of *in-situ* GPP measurements may influence our results. However, the full mechanism of how topography affects GPP is tremendously complex and out of the scope of our study. The topographic effects embedded in GPP measurements were not considered in our study. In fact, several studies showed the topographic effects on GPP are not significant [48-50]. Further dedicated studies are need to better understand the GPP topographic effects and possible scale dependences.

Previous studies indicate that the selection of the evaluation criteria influences the evaluation results of topographic correction [51]. We employed a widely used topographic correction evaluation method, i.e., the correlation analysis with the cosine of local solar incident angle [26], to assess the performance of the TCNIRv in reducing the topographic effect. However, this evaluation implicitly assumes the land cover distribution is independent of slope orientation [52]. Obviously, this assumption is not always valid in real world, given that topography influences vegetation's hydrothermal conditions. Therefore, residual correlation as is expected, even after a perfect topographic correction. Given this limitation, it may be worthwhile to implement the multi-criteria evaluation which would provide a comprehensive assessment result [26, 27, 53].

In addition, the selection of DEM products is also critical for topographic correction [54]. Previous studies [55, 56] demonstrated that AW3D30 DEM outperformed other commonly used DEM products, including SRTM and ASTER GDEM, in characterizing topography over mountainous areas. However, direct comparison revealed a high consistence among them in our study area (R^2 > 0.99, see Fig. A2). Therefore, AW3D30 DEM is a reliable selection for our study.

In rugged areas, the downward irradiance received by a slopped surface incorporates solar-direct, sky-diffuse and terrain-reflected radiance [57]. Their relative proportion varies with time and weather [58]. For example, in winter and early spring, the sky-diffuse and terrain-reflected radiance proportion dominate solar-direct [58]. However, only the solar-direct radiance component is considered in TCNIRv, and this would cause relative more uncertainty in winter and early spring. In addition, Dechant *et al.* [59] demonstrated that NIRvP, the product of NIRv and downward photosynthetically active radiation (PAR), was a more robust proxy for plant photosynthesis. This finding also highlighted the importance of accurate characterization of downward irradiance over mountainous areas [60, 61]. In future work, the characterization of downward irradiance (i.e., account for the influence of sky-diffuse and terrain-reflected radiance) would be incorporated into TCNIRv to further improve its performance in GPP monitoring over mountainous areas.

VI. Conclusions

This is the first study to propose a topographic correction formulation for the near-infrared reflectance of vegetation (NIRv). The topographically-corrected NIRv, called TCNIRv, was demonstrated to be a robust proxy of GPP over mountainous areas. TCNIRv adopted a topographic normalization conversion factor derived from path length correction (PLC) to reduce topographic effects on NIRv. Multiple Landsat-8 Operational Land Imager images and *in-situ* GPP measurements from 2014 to 2018 were combined to evaluate the proposed TCNIRv. The TCNIRv was comparable to or even outperformed NDVI and GNDVI in reducing topographic effects. In addition, TCNIRv improved these VIs as well as the original NIRv in tracking the seasonal variations of GPP over mountainous areas (R^2 = 0.90 and RMSE = 1.40 $gCm^{-2}d^{-1}$ for TCNIRv compared to R^2 = 0.71 and RMSE = 2.47 $gCm^{-2}d^{-1}$ for NIRv). The solid physical basis of TCNIRv with no empirical parameters and simple formulation makes it a useful tool for temporally and spatially consistent vegetation monitoring over mountainous areas.

Appendix

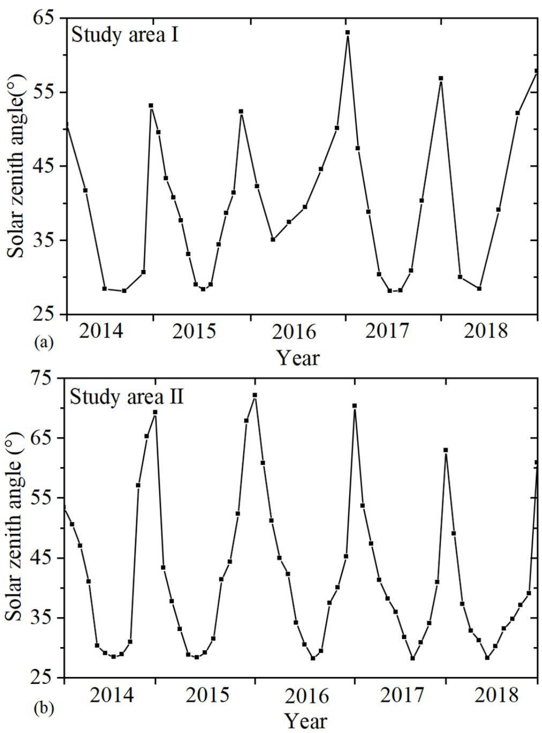

Fig. A1. The temporal profile of the solar zenith angle in study area I and II.

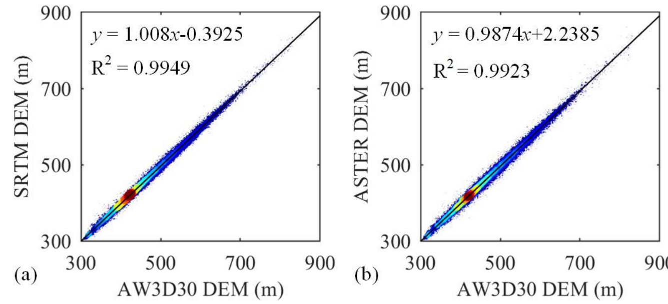

Fig. A2. The comparison of SRTM DEM (a) and ASTER DEM (b) with AW3D30 DEM. The solid lines are the regressed results.

References

[1] C. Wu, J. W. Munger, Z. Niu, and D. Kuang, "Comparison of multiple models for estimating gross primary production using MODIS and eddy covariance data in Harvard Forest," *Remote Sens. Environ.,* vol. 114, no. 12, pp. 2925-2939, 2010, doi: 10.1016/j.rse.2010.07.012.

[2] R. Richter, T. Kellenberger, and H. Kaufmann, "Comparison of Topographic Correction Methods," *Remote Sens.,* vol. 1, no. 3, pp. 184-196, 2009, doi: 10.3390/rs1030184.

[3] J. Wen *et al.*, "Characterizing Land Surface Anisotropic Reflectance over Rugged Terrain: A Review of Concepts and Recent Developments," *Remote Sens.,* vol. 10, no. 3, 2018, doi: 10.3390/rs10030370.

[4] P. J. Sellers *et al.*, "Modeling the Exchanges of Energy, Water, and Carbon Between Continents and the Atmosphere," *Science,* vol. 275, no. 5299, p. 502, 1997, doi: 10.1126/science.275.5299.502.

[5] J. L. Monteith, "Solar Radiation and Productivity in Tropical Ecosystems," *J. Appl. Ecol.,* vol. 9, no. 3, pp. 747-766, 1972, doi: 10.2307/2401901.

[6] A. Hamann and T. L. Wang, "Models of climatic normals for genecology and climate change studies in British Columbia," *Agricult. Forest Meteorol.,* vol. 128, no. 3-4, pp. 211-221, 2005, doi: 10.1016/j.agrformet.2004.10.004.

[7] A. C. Almeida and J. J. Landsberg, "Evaluating methods of estimating global radiation and vapor pressure deficit using a dense network of automatic weather stations in coastal Brazil," *Agricult. Forest Meteorol.,* vol. 118, no. 3-4, pp. 237-250, 2003, doi: 10.1016/s0168-1923(03)00122-9.

[8] J. W. Rouse, Jr., R. H. Haas, J. A. Schell, and D. W. Deering, "Monitoring Vegetation Systems in the Great Plains with Erts," vol. 351, 1974, p. 309.

[9] S. Piao, P. Friedlingstein, P. Ciais, N. Viovy, and J. Demarty, "Growing season extension and its impact on terrestrial carbon cycle in the Northern Hemisphere over the past 2 decades," *Glob. biogeochem. cycles.,* vol. 21, no. 3, pp. n/a-n/a, 2007, doi: 10.1029/2006gb002888.

[10] Y. Liu *et al.*, "Improved modeling of land surface phenology using MODIS land surface reflectance and temperature at evergreen needleleaf forests of central North America," *Remote Sens. Environ.,* vol. 176, pp. 152-162, 2016, doi: 10.1016/j.rse.2016.01.021.

[11] A. Huete, K. Didan, T. Miura, E. P. Rodriguez, X. Gao, and L. G. Ferreira, "Overview of the radiometric and biophysical performance of the MODIS vegetation indices," *Remote Sens. Environ.,* vol. 83, no. 1, pp. 195-213, 2002/11/01/ 2002, doi: https://doi.org/10.1016/S0034-4257(02)00096-2.

[12] C. Wu *et al.*, "Land surface phenology derived from normalized difference vegetation index (NDVI) at global FLUXNET sites," *Agricult. Forest Meteorol.,* vol. 233, pp. 171-182, 2017/02/15/ 2017, doi: https://doi.org/10.1016/j.agrformet.2016.11.193.

[13] G. Yin, A. Verger, I. Filella, A. Descals, and J. Peñuelas, "Divergent Estimates of Forest Photosynthetic Phenology Using Structural and Physiological Vegetation Indices," *Geophys. Res. Lett.,* https://doi.org/10.1029/2020GL089167 vol. 47, no. 18, p. e2020GL089167, 2020/09/28 2020, doi: https://doi.org/10.1029/2020GL089167.

[14] A. A. Gitelson *et al.*, "Relationship between gross primary production and chlorophyll content in crops: Implications for the synoptic monitoring of vegetation productivity," *J. Geophys. Res.,* vol. 111, no. D8, 2006, doi: 10.1029/2005jd006017.

[15] G. Badgley, L. D. L. Anderegg, J. A. Berry, and C. B. Field, "Terrestrial gross primary production: Using NIRV to scale from site to globe," *Glob*

Chang Biol, vol. 25, no. 11, pp. 3731-3740, Nov 2019, doi: 10.1111/gcb.14729.

[16] D. D. Baldocchi *et al.*, "Outgoing Near-Infrared Radiation From Vegetation Scales With Canopy Photosynthesis Across a Spectrum of Function, Structure, Physiological Capacity, and Weather," *J. Geophys. Res. Biogeosci.,* vol. 125, no. 7, 2020, doi: 10.1029/2019jg005534.

[17] G. Badgley, C. B. Field, and J. A. Berry, "Canopy near-infrared reflectance and terrestrial photosynthesis," *Sci Adv,* vol. 3, no. 3, p. e1602244, Mar 2017, doi: 10.1126/sciadv.1602244.

[18] R. Chen, G. Yin, G. Liu, J. Li, and A. Verger, "Evaluation and Normalization of Topographic Effects on Vegetation Indices," *Remote Sens.,* vol. 12, no. 14, 2020, doi: 10.3390/rs12142290.

[19] J. Wen, Q. Liu, Q. Liu, Q. Xiao, and X. Li, "Parametrized BRDF for atmospheric and topographic correction and albedo estimation in Jiangxi rugged terrain, China," *Int. J. Remote Sens.,* vol. 30, no. 11, pp. 2875-2896, 2009, doi: 10.1080/01431160802558618.

[20] W. Fan, J. Chen, W. Ju, and G. Zhu, "GOST: A Geometric-Optical Model for Sloping Terrains," *IEEE Trans. Geosci. Remote Sens.,* vol. 52, pp. 5469-5482, 09/01 2014, doi: 10.1109/TGRS.2013.2289852.

[21] G. Yin, A. Li, W. Zhao, H. Jin, J. Bian, and S. Wu, "Modeling Canopy Reflectance Over Sloping Terrain Based on Path Length Correction," *IEEE Trans. Geosci. Remote Sens.,* vol. 55, no. 8, pp. 4597-4609, 2017, doi: 10.1109/tgrs.2017.2694483.

[22] P. M. Teillet, B. Guindon, and D. G. Goodenough, "On the Slope-Aspect Correction of Multispectral Scanner Data," *Can. J. Remote. Sens.,* vol. 8, no. 2, pp. 84-106, 1982/12/01 1982, doi: 10.1080/07038992.1982.10855028.

[23] D. Gu and A. Gillespie, "Topographic Normalization of Landsat TM Images of Forest Based on Subpixel Sun–Canopy–Sensor Geometry," *Remote Sens. Environ.,* vol. 64, no. 2, pp. 166-175, 1998/05/01/ 1998, doi: https://doi.org/10.1016/S0034-4257(97)00177-6.

[24] J. Dymond and J. D. Shepherd, "Correction of the topographic effect in remote sensing," *IEEE Trans. Geosci. Remote Sens.,* vol. 37, pp. 2618-2619, 10/01 1999, doi: 10.1109/36.789656.

[25] S. A. Soenen, D. R. Peddle, and C. A. Coburn, "SCS+C: a modified Sun-canopy-sensor topographic correction in forested terrain," *IEEE Trans. Geosci. Remote Sens.,* vol. 43, no. 9, pp. 2148-2159, 2005, doi: 10.1109/TGRS.2005.852480.

[26] I. Sola, M. González-Audícana, and J. Álvarez-Mozos, "Multi-criteria evaluation of topographic correction methods," *Remote Sens. Environ.,* vol. 184, pp. 247-262, 2016, doi: 10.1016/j.rse.2016.07.002.

[27] G. Yin *et al.*, "PLC: A simple and semi-physical topographic correction method for vegetation canopies based on path length correction," *Remote Sens. Environ.,* vol. 215, pp. 184-198, 2018/09/15/ 2018, doi: https://doi.org/10.1016/j.rse.2018.06.009.

[28] H. Reese and H. Olsson, "C-correction of optical satellite data over alpine vegetation areas: A comparison of sampling strategies for determining the empirical c-parameter," *Remote Sens. Environ.,* vol. 115, no. 6, pp. 1387-1400, 2011, doi: 10.1016/j.rse.2011.01.019.

[29] G. Yin, L. Ma, W. Zhao, Y. Zeng, B. Xu, and S. Wu, "Topographic Correction for Landsat 8 OLI Vegetation Reflectances Through Path Length Correction: A Comparison Between Explicit and Implicit Methods," *IEEE Trans. Geosci. Remote Sens.,* pp. 1-13, 2020, doi: 10.1109/tgrs.2020.2987985.

[30] G. Yin *et al.*, "Derivation of temporally continuous LAI reference maps through combining the LAINet observation system with CACAO," *Agricult. Forest Meteorol.,* vol. 233, pp. 209-221, 2017, doi: 10.1016/j.agrformet.2016.11.267.

[31] Y. Zeng, G. Badgley, B. Dechant, Y. Ryu, M. Chen, and J. A. Berry, "A practical approach for estimating the escape ratio of near-infrared solar-induced chlorophyll fluorescence," *Remote Sens. Environ.,* vol. 232, 2019, doi: 10.1016/j.rse.2019.05.028.

[32] S. Etzold *et al.*, "The Carbon Balance of Two Contrasting Mountain Forest Ecosystems in Switzerland: Similar Annual Trends, but Seasonal Differences," *Ecosystems,* vol. 14, no. 8, pp. 1289-1309, 2011, doi: 10.1007/s10021-011-9481-3.

[33] J. Chen, P. Jönsson, M. Tamura, Z. Gu, B. Matsushita, and L. Eklundh, "A simple method for reconstructing a high-quality NDVI time-series data set based on the Savitzky–Golay filter," *Remote Sens. Environ.,* vol. 91, no. 3-4, pp. 332-344, 2004, doi: 10.1016/j.rse.2004.03.014.

[34] A. Savitzky and M. J. E. Golay, "Smoothing and Differentiation of Data by Simplified Least Squares Procedures," *Anal. Chem.,* vol. 36, no. 8, pp. 1627-1639, 1964/07/01 1964, doi: 10.1021/ac60214a047.

[35] L. Eklundh and P. Jönsson, "TIMESAT 3.3 with seasonal trend decomposition and parallel processing - Software Manual," pp. Lund University, 92 pp, 2017.

[36] N. Gorelick, M. Hancher, M. Dixon, S. Ilyushchenko, D. Thau, and R. Moore, "Google Earth Engine: Planetary-scale geospatial analysis for everyone," *Remote Sens. Environ.,* vol. 202, pp. 18-27, 2017, doi: 10.1016/j.rse.2017.06.031.

[37] E. Vermote, J.-C. Roger, B. Franch, and S. Skakun, *LaSRC (Land Surface Reflectance Code): Overview, application and validation using MODIS, VIIRS, LANDSAT and Sentinel 2 data's*. 2018, pp. 8173-8176.

[38] Z. Zhu, S. Wang, and C. E. Woodcock, "Improvement and expansion of the Fmask algorithm: cloud, cloud shadow, and snow detection for Landsats 4–7, 8, and Sentinel 2 images," *Remote Sens. Environ.,* vol. 159, pp. 269-277, 2015, doi: 10.1016/j.rse.2014.12.014.

[39] O. Yuji, H. Masaru, and K. Ichida, "PRISM: a panchromatic three-line sensor for mapping onboard ALOS," in *Proc.SPIE*, 1998, vol. 3498, doi: 10.1117/12.333627. [Online]. Available: https://doi.org/10.1117/12.333627

[40] T. Tadono *et al.*, "GENERATION OF THE 30 M-MESH GLOBAL DIGITAL SURFACE MODEL BY ALOS PRISM," *ISPRS - International Archives of the Photogrammetry, Remote Sensing and Spatial Information Sciences,* vol. XLI-B4, pp. 157-162, 06/13 2016, doi: 10.5194/isprs-archives-XLI-B4-157-2016.

[41] B. Matsushita, W. Yang, J. Chen, Y. Onda, and G. Qiu, "Sensitivity of the Enhanced Vegetation Index (EVI) and Normalized Difference Vegetation Index (NDVI) to Topographic Effects: A Case Study in High-density Cypress Forest," *Sensors,* vol. 7, no. 11, 2007, doi: 10.3390/s7112636.

[42] S. Wang, Y. Zhang, W. Ju, B. Qiu, and Z. Zhang, "Tracking the seasonal and inter-annual variations of global gross primary production during last four decades using satellite near-infrared reflectance data," *Sci Total Environ,* vol. 755, no. Pt 2, p. 142569, Sep 30 2020, doi: 10.1016/j.scitotenv.2020.142569.

[43] A. A. Gitelson, Y. J. Kaufman, and M. N. Merzlyak, "Use of a green channel in remote sensing of global vegetation from EOS-MODIS," *Remote Sens. Environ.,* vol. 58, no. 3, pp. 289-298, 1996/12/01/ 1996, doi: https://doi.org/10.1016/S0034-4257(96)00072-7.

[44] N. K. Rühr and W. Eugster, "Soil respiration fluxes and carbon sequestration of two mountain forests in Switzerland. Report for the Federal Office for the Environment," ETH, 2009. [Online]. Available: http://hdl.handle.net/20.500.11850/157922

[45] J. M. Chen, X. Chen, and W. Ju, "Effects of vegetation heterogeneity and surface topography on spatial scaling of net primary productivity," *Biogeosciences,* vol. 10, no. 7, pp. 4879-4896, 2013, doi: 10.5194/bg-10-4879-2013.

[46] Z. Liao, B. He, and X. Quan, "Modified enhanced vegetation index for reducing topographic effects," *J. Appl. Remote. Sens.,* vol. 9, p. 096068, 03/27 2015, doi: 10.1117/1.JRS.9.096068.

[47] J. Kim *et al.*, "HydroKorea and CarboKorea: cross-scale studies of ecohydrology and biogeochemistry in a heterogeneous and complex forest catchment of Korea," *Ecol. Res.,* vol. 21, no. 6, pp. 881-889, 2006, doi: 10.1007/s11284-006-0055-3.

[48] X. Xie and A. Li, "Development of a topographic-corrected temperature and greenness model (TG) for improving GPP estimation over mountainous areas," *Agricult. Forest Meteorol.,* vol. 295, 2020, doi: 10.1016/j.agrformet.2020.108193.

[49] X. Xie and A. Li, "An Adjusted Two-Leaf Light Use Efficiency Model for Improving GPP Simulations Over Mountainous Areas," *Journal of Geophysical Research: Atmospheres,* vol. 125, no. 13, 2020, doi: 10.1029/2019jd031702.

[50] T. Hwang, S. Kang, J. Kim, Y. Kim, D. Lee, and L. Band, "Evaluating drought effect on MODIS Gross Primary Production (GPP) with an eco-hydrological model in the mountainous forest, East Asia," *Global Change Biol.,* vol. 14, no. 5, pp. 1037-1056, 2008, doi: 10.1111/j.1365-2486.2008.01556.x.

[51] I. Sola, M. Gonzalez-Audicana, J. Alvarez-Mozos, and J. L. Torres, "Synthetic Images for Evaluating Topographic Correction Algorithms," *IEEE Trans. Geosci. Remote Sens.,* vol. 52, no. 3, pp. 1799-1810, 2014, doi: 10.1109/tgrs.2013.2255296.

[52] S. Hantson and E. Chuvieco, "Evaluation of different topographic correction methods for Landsat imagery," *Int. J. Appl. Earth Obs. Geoinf.,* vol. 13, no. 5, pp. 691-700, 2011, doi: 10.1016/j.jag.2011.05.001.

[53] K. Hurni, J. Van Den Hoek, and J. Fox, "Assessing the spatial, spectral, and temporal consistency of topographically corrected Landsat time series composites across the mountainous forests of Nepal," *Remote Sens.*

This article has been accepted for publication in IEEE Transactions on Geoscience and Remote Sensing. This is the author's version which has not been fully edited and content may change prior to final publication. Citation information: DOI 10.1109/TGRS.2022.3149655

Environ., vol. 231, p. 111225, 2019/09/15/ 2019, doi: https://doi.org/10.1016/j.rse.2019.111225.

[54] H. Adhikari, J. Heiskanen, E. E. Maeda, and P. K. E. Pellikka, "The effect of topographic normalization on fractional tree cover mapping in tropical mountains: An assessment based on seasonal Landsat time series," *Int. J. Appl. Earth Obs. Geoinf.,* vol. 52, pp. 20-31, 2016, doi: 10.1016/j.jag.2016.05.008.

[55] I. V. Florinsky, T. N. Skrypitsyna, and O. S. Luschikova, "Comparative accuracy of the AW3D30 DSM, ASTER GDEM, and SRTM1 DEM: A case study on the Zaoksky testing ground, Central European Russia," *Remote Sensing Letters,* vol. 9, no. 7, pp. 706-714, 2018, doi: 10.1080/2150704x.2018.1468098.

[56] U. Alganci, B. Besol, and E. Sertel, "Accuracy Assessment of Different Digital Surface Models," *ISPRS International Journal of Geo-Information,* vol. 7, no. 3, 2018, doi: 10.3390/ijgi7030114.

[57] C. Proy, D. Tanré, and P. Y. Deschamps, "Evaluation of topographic effects in remotely sensed data," *Remote Sens. Environ.,* vol. 30, no. 1, pp. 21-32, 1989/10/01/ 1989, doi: https://doi.org/10.1016/0034-4257(89)90044-8.

[58] Y. Chen, A. Hall, and K. N. Liou, "Application of three-dimensional solar radiative transfer to mountains," *J. Geophys. Res.,* vol. 111, no. D21, 2006, doi: 10.1029/2006jd007163.

[59] B. Dechant *et al.*, "NIRVP: A robust structural proxy for sun-induced chlorophyll fluorescence and photosynthesis across scales," *Remote Sens. Environ.,* vol. 268, p. 112763, 2022/01/01/ 2022, doi: https://doi.org/10.1016/j.rse.2021.112763.

[60] W. Wang, G. Yin, W. Zhao, F. Wen, and D. Yu, "Spatial Downscaling of MSG Downward Shortwave Radiation Product Under Clear-Sky Condition," *IEEE Trans. Geosci. Remote Sens.,* vol. 58, no. 5, pp. 3264-3272, 2020, doi: 10.1109/tgrs.2019.2951699.

[61] W. Zhao, X. Li, W. Wang, F. Wen, and G. Yin, "DSRC: An Improved Topographic Correction Method for Optical Remote-Sensing Observations Based on Surface Downwelling Shortwave Radiation," *IEEE Trans. Geosci. Remote Sens.,* pp. 1-15, 2021, doi: 10.1109/TGRS.2021.3083754.

Rui Chen received the B.S. degree in surveying and mapping engineering from the China University of Petroleum (East China), Qingdao, China, in 2019. He is pursuing the Ph.D. degree with the Faculty of Geosciences and Environmental Engineering, Southwest Jiaotong University, Chengdu, China.

His research interests include topographic correction for optical remote sensing images and vegetation remote sensing.

Gaofei Yin (Senior Member, IEEE) received the Ph.D. degree from the Institute of Remote Sensing and Digital Earth, Chinese Academy of Sciences, Beijing, China, in 2015.

From 2019 to 2021, he worked as a Marie Skłodowska-Curie Individual Fellow at the Global Ecology Unit, Center for Ecological Research and Forestry Applications, Barcelona, Spain. He is currently a professor in the Faculty of Geosciences and Environmental Engineering, Southwest Jiaotong University, Chengdu, China. He also serves as an associated editor for IEEE Geoscience and Remote Sensing Letters. His current research interests include vegetation remote sensing, and global change ecology.

Wei Zhao (Senior Member, IEEE) received the B.S. degree in Geographic Information System from Beijing Normal University, Beijing, China, in 2006 and the Ph.D. degree in Cartography and Geographic Information System from Institute of Geographic Sciences and Natural Resources Research, Chinese Academy of Sciences (CAS), Beijing, China, in 2012.

Since 2012, he is with the Institute of Mountain Hazards and Environment (IMHE), CAS, Chengdu, China. Currently, he is a youth professor with IMHE. His research field is mountain quantitative remote sensing with special focuses on land surface energy fluxes and soil moisture estimation, spatial scale effect on remote sensing data, and thermal environment monitoring.

Baodong Xu (Member, IEEE) received the Ph.D. degree from the Institute of Remote Sensing and Digital Earth, Chinese Academy of Sciences, in 2018.

Since 2018, he has been an Associate Professor with the Macro Agriculture Research Institute, College of Resources and Environment, Huazhong Agricultural University, Wuhan, China. His research interests include biophysical variables estimation, validation of remote sensing products, and remote sensing applications in agriculture.

Yelu Zeng (Member, IEEE) received the B.S. degree in remote sensing from Wuhan University, Wuhan, China, in 2011, and the Ph.D. degree from the Institute of Remote Sensing and Digital Earth, Chinese Academy of Sciences, Beijing, China, in 2016.

He worked as a Post-doctoral Fellow at Carnegie Institution for Science in Stanford, CA, USA during July, 2017 to Dec, 2019, a Post Doctorate Research Associate at Joint Global Change Research Institute of the Pacific Northwest National Laboratory, MD, USA during Jan, 2020 to Jan, 2021, and an Assistant Scientist at Department of Forest and Wildlife Ecology at the University of Wisconsin-Madison, WI, USA during Jan, 2021 to Oct, 2021. He is currently a Professor at College of Land Science and Technology, China Agricultural University, Beijing, 100083, China. His research interests include 3-D radiative transfer modeling over vegetation canopies and solar-induced chlorophyll fluorescence (SIF).

Guoxiang Liu received the B.E. degree in surveying engineering from the East China Institute of Geology, Jiangxi, China, in 1991, the M.E. degree in geomatics from the Southwest Jiaotong University, Chengdu, China, in 1994, and the Ph.D.degree in remote sensing from The Hong Hong Ploytechnic University, Hong Kong, China, in 2003.

He is currently a Professor with the Department of Remote Sensing and Geospatial Information Engineering, Southwest Jiaotong University. From September 2005 to September 2006, he was a Visiting Scholar and conducted research on InSAR with Dr. S. M. Buckley with the Department of Aerospace Engineering and Engineering Mechanics, The University of Texas at Austin, TX, USA. He is the author of three books, more than 170 articles, and holds twelve patents. His current research interests include InSAR, PSI, radargrammetry and digital photogrammetry for regional mapping topography, and deformation.

Aleixandre Verger received the PhD in Physics from the University of Valencia in 2008. He is currently a researcher at the Desertification Research Centre CIDE-CSIC and at CREAF-CSIC-UAB. His research interests include the development of remote sensing methods for monitoring essential vegetation variables in the fields of environment, ecology, agriculture, and global change. He has been leading the development of the operational algorithms for the retrieval of biophysical variables such as leaf area index and fraction of absorbed photosynthetically active radiation from satellite data within the Copernicus Global Land and Copernicus Climate Change Services, among others.